Liquid Crystals
Publication details, including instructions for authors and subscription information:
http://www.informaworld.com/smpp/title~content=t713926090

Multiple scattering effects in polymer dispersed liquid crystals

J. R. Kelly[a]; Wei Wu[a]
[a] Department of Physics, Liquid Crystal Institute, Kent State University, Kent, Ohio, U.S.A.

To cite this Article Kelly, J. R. and Wu, Wei(1993) 'Multiple scattering effects in polymer dispersed liquid crystals', Liquid Crystals, 14: 6, 1683 — 1694
To link to this Article: DOI: 10.1080/02678299308027708
URL: http://dx.doi.org/10.1080/02678299308027708

LIQUID CRYSTALS, 1993, VOL. 14, NO. 6, 1683–1694

Multiple scattering effects in polymer dispersed liquid crystals

by J. R. KELLY* and WEI WU
Liquid Crystal Institute and Department of Physics, Kent State University, Kent, Ohio 44242, U.S.A.

We have measured the angular distribution of light scattered from PDLC films with micron-sized droplets as a function of film thickness and applied voltage. We find that a single scattering picture does not give a good description of the observed scattered intensity. In particular, the intensity falls off much more weakly with scattering angle than one would predict from the anomalous diffraction cross-section calculated by Zumer. We present a simple model for describing double and higher order scattering events that gives a better quantitative description of the experimental observations. The model can be combined with a model for the switching behaviour of PDLC films to describe the scattering as a function of the applied voltage.

1. Introduction

Polymer dispersed liquid crystals (PDLC) films, consisting of micron-sized nematic droplets dispersed in a polymer binder, have rather dramatic light scattering properties [1, 2, 3]. These films can be switched from an opaque to a clear state by an applied field if the ordinary index of the liquid crystal is matched to the index of the polymer. Because of this property, these films have found a number of applications. PDLC films are particularly suited to projection displays, where high light throughput and excellent contrast ratios can be achieved [4, 5].

For an ideal projection display, the collection optics would be f/∞, i.e. only unscattered light would be collected. However, in real systems, f numbers are much smaller: $f/10$ is typical. If the light is strongly scattered in the forward direction, this will have a dramatic impact on the optical performance, in both contrast and speed [6]. To optimize this performance, it is important to have a detailed understanding of the scattering characteristics of PDLC films. Here we describe the results of a study of the angular distribution of light scattered from ultraviolet-cured polymer/liquid crystal dispersions.

There are three important effects that govern the distribution of the scattered light. Foremost is the scattering by a single droplet. Second, there are coherent effects associated with the interference between waves scattered from different droplets; and finally, multiple scattering events are significant when the droplet density or film thickness is large. When we consider the total scattering cross-section, only the first effect plays a major role; the other two influence the distribution of the scattered light, but have less impact on the amount of scattered light [7]. For this reason, a single scattering picture gives a good description of the film transmittance [8]. However, when considering the angular distribution of the scattered light, we can anticipate that interference and multiple scattering will be important.

Zumer has studied, theoretically, the light scattering from a single spherical birefringent droplet [9, 10]. For droplets much smaller than the wavelength of the

*Author for correspondence.

0267–8292/93 $10·00

light, the Rayleigh-Gans approximation gives a good description of the scattering, while, for droplets comparable in size to the wavelength, the anomalous diffraction approach (ADA) is more appropriate. In either case, the scattering is strongly dependent on the nematic director configuration in the droplet.

The interference between droplets depends on their spatial distribution, as described by the structure factor, or the related pair correlation function. Presumably, if one knows the spatial distribution of the droplets, as deduced, for example, from scanning electron micrographs (SEM), then the structure factor can be determined. At present, no such result exists for any PDLC system. However, it is expected to be strongly dependent on the phase separation process. It is doubtful that the structure factor will be the same for different systems or different preparations. Indeed, the structure factor can provide useful information regarding the droplet formation process [11].

In PDLC films formed by phase separation techniques, the droplet density is relatively high: volume fractions ranging between 0·3 and 0·5 are common. For such densities, multiple scattering is expected to play a major role in determining the scattering profile. For multiple scattering we can anticipate that coherence effects are mitigated, leading to scattering that can be described primarily by the superposition of scattered light intensities.

Before looking at the results of the scattering experiments, we will describe a simple model of the light scattering, including multiple scattering effects. It is futile to attempt describing the scattering of light by a PDLC in a completely rigorous way.

2. Scattering model

To model the light scattering by a PDLC film, we make the following assumptions:

(1) Single scattering can be treated by the ADA.
(2) Droplets are spherical and the same size. Including a droplet size distribution is straightforward, but is not necessary for our purposes here [12].
(3) Droplets have a uniform director configuration. This, along with (2) permits the use of the ADA results of Zumer for birefringent spheres. The symmetry axis is specified by a droplet director, $\hat{\mathbf{N}}_d$, that lies along the axis of uniaxial symmetry.
(4) In the absence of an applied field, the droplet directors are uniformly distributed over all solid angles. When a field is applied, each director makes an angle θ with the applied field according to:

$$\cos^2\theta = \frac{1}{2} + \frac{1}{2}\cdot\frac{e^2 - 1 + \cos^2\beta}{\sqrt{((e^2-1)^2 + 4e^2\cos^2\beta)}}, \tag{1}$$

where β is the angle that the droplet director makes with the field direction (the film normal) in the absence of an applied field; e is a reduced field that is proportional to the applied field. Equation (1) is derived from a phenomenological torque balance equation that balances the field and elastic contributions to the free energy of a droplet [13].
(5) The film is index matched; i.e. the ordinary index of refraction of the liquid crystal and the index of refraction of the polymer are the same.

To fix ideas more firmly, we will consider coherent, linearly polarized, monochromatic light with wavevector $\mathbf{k}$ incident normal to the film plane. The outgoing scattered wave has a wavevector $\mathbf{k}'$ that makes an angle δ with $\mathbf{k}$. The electric vector of the polarized light makes an angle α_0 with the plane defined by $\mathbf{N}_d$ and $\mathbf{k}$.

2.1. *Single scattering*

According to Zumer [7], the effective differential cross-section for single scattering is

$$\frac{d\sigma}{d\Omega} = F(\mathbf{q}) \left\langle \frac{d\sigma}{d\Omega}(\theta, \alpha_0) \right\rangle_{\text{film}} \tag{2}$$

where $F(\mathbf{q})$ is the structure factor with $\mathbf{q} \equiv \mathbf{k} - \mathbf{k}'$. $\langle \ldots \rangle_{\text{film}}$ means the average over the individual droplet cross-sections. This average involves an average over droplet director orientations with respect to both the incident wave vector and the incident field. To find this average, we start with the differential cross-section for a single droplet, of radius R, with uniform director field

$$\frac{d\sigma}{d\Omega}(\theta, \alpha_0) = \frac{k^2 R^4}{4} |H(v_e, kR \sin \delta)|^2 \cos^2 \alpha_0. \tag{3}$$

H is a complex function of its arguments

$$H(v, z) = \int_0^1 \{1 - \exp [iv(1-x^2)^{1/2}]\} J_0(xz) x \, dx. \tag{4}$$

J_0 is the Bessel function of zeroth order. The dependence of the cross-section on θ enters implicitly into Equation (3) through v_e

$$v_e = 2kR \left[\frac{n_e(\theta)}{n_o} - 1 \right], \tag{5}$$

where n_o is the ordinary index of refraction of the liquid crystal and $n_e(\theta)$ is the effective extraordinary index for polarization in the $\mathbf{N}_d$–$\mathbf{k}$ plane:

$$n_e(\theta) = \left[\frac{\cos^2(\theta)}{n_o^2} + \frac{\sin^2(\theta)}{n_e^2} \right]^{-1/2}. \tag{6}$$

The film averaged differential cross-section is shown in figure 1 as a function of δ, for a range of (reduced) applied fields, e. The film order parameter, S_f, is also given for reference. S_f is a measure of how well the droplet directors are aligned by the applied field and is defined by [3]

$$S_f = \frac{3}{2} \langle \cos^2 \theta \rangle_{\text{film}} - \frac{1}{2}. \tag{7}$$

As one expects, the film-averaged cross-section decreases with the applied field. While it is not evident from the equations, the film averaged cross-section has nearly the same profile for all applied fields (see figure 2). Therefore, for single scattering, when a field is applied, the angular distribution of the scattered light remains the same; only the intensity changes.

2.2. *Multiple scattering*

A rigorous solution for light scattering by a distribution of spheres is not at hand, even for the case when the medium is isotropic [14]. Still, one could, in

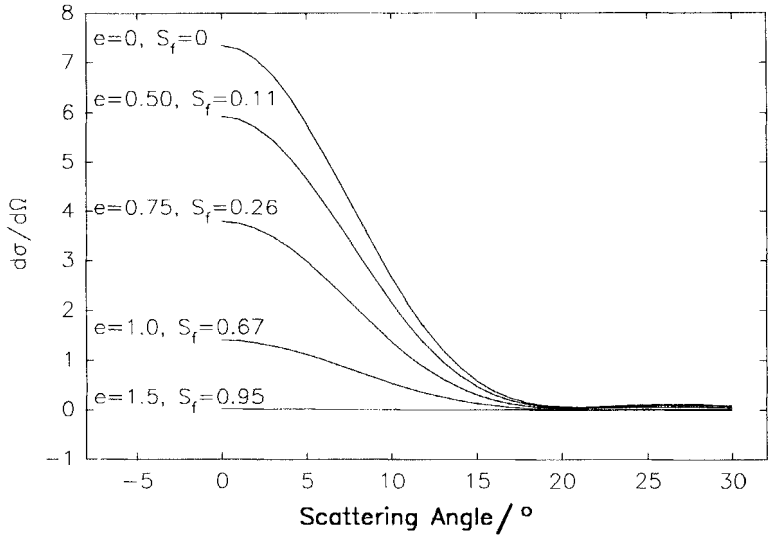

Figure 1. Theoretical single scattering patterns for different applied fields.

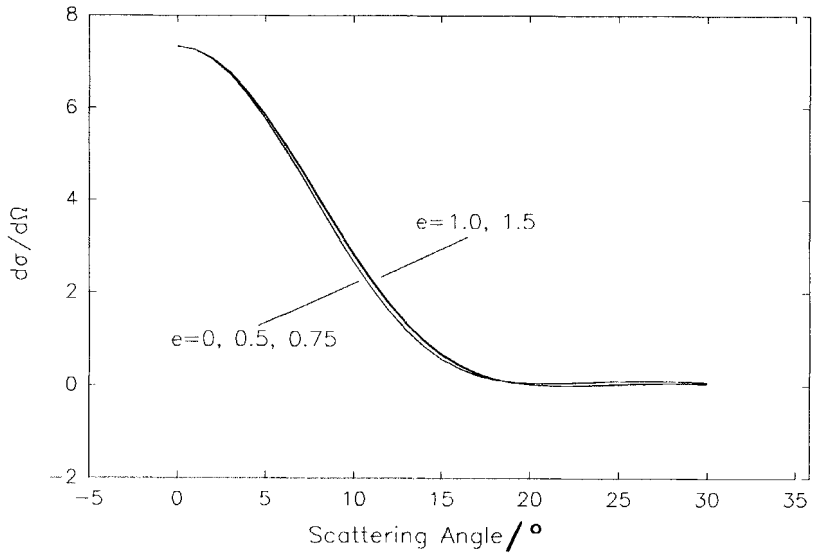

Figure 2. Theoretical single scattering patterns for different applied fields, all scaled to give the same maximum for $d\sigma/d\Omega$.

principle, find at least an approximate solution by some perturbative scheme, such as successive approximation. In this approach, to the lowest order, each droplet sees the incoming plane wave and acts as an isolated scatterer. These lowest order scattered waves are then superposed with the incident field at each point, providing a first order corrected field. Repetition of this algorithm would lead to successively better approximations of the scattered field.

If we imagine applying this approach to a collection of micron-sized nematic droplets, the perturbed fields would be nearly zero except in the forward direction; a droplet will multiply scattered light only if it lies in or near the geometrical shadow of other droplets. This motivates in part the following model of the multiple scattering.

Initially, we ignore coherent and interference effects except those accounted for in the previous section. In this way, we envision the multiple scattering as a sequence of independent photon scattering events. When a photon is scattered, the probability of scattering through a particular angle is governed by the effective single droplet differential cross-section.

To proceed, we need the probability that a photon is scattered n times. We choose an ansatz that has intuitive appeal and demonstrates the appropriate behaviour in the limit of low droplet densities. The probability that a photon is scattered n times is taken equal to the probability that a ray passing normally through the film will encounter n scatterers, whose geometrical cross-sections are taken equal to the film-averaged total scattering cross-section. (This will underestimate the actual number of encounters, but for strong forward scattering the mean path length is only slightly longer due to the scattering.) If the droplets are randomly distributed, this probability is just the normalized Poisson distribution

$$p(n;\, a)=\frac{a^n}{n!}\exp(-a). \tag{8}$$

Noting that $p(0;a)$ is the fraction of unscattered light, we identify it with the film transmittance, T, according to Lambert's Law; so

$$p(n;\, T)=\frac{(-\ln T)^n}{n!}T. \tag{9}$$

These probabilities are shown in figure 3 for the first few n. In this case, if the droplet density is ρ and the film thickness is d

$$a=-\ln T=\rho\sigma_f d, \tag{10}$$

where σ_f is the film-averaged total cross-section.

As a consequence of equations (9) and (10) we observe that once the film transmittance is specified, the scattering profile is uniquely determined. Or, as a corollary: for fixed kR, the angular distribution of scattered light depends only upon the film transmittance, not independently on the film thickness or the applied voltage.

A FORTRAN program was developed to calculate the multiple scattering patterns. Figure 4 shows the flow chart of the program. The single scattering patterns for $kR=13$ can be fitted to an analytical function in the form of $a\cdot\exp(-b\cdot\theta^2)$, where a is a scaling factor, and $b=0{\cdot}0104$ if θ is expressed in degrees. We limit the multiple scattering order to the 25th, which suffices for the transmittance down to 0·01 per cent. After the total number of iterations is specified, the number of iterations for each multiple scattering order is determined by equation (9). Inside each iteration, the polar angle θ is randomly generated according to the single scattering pattern, and the azimuthal angle ϕ follows a uniform random

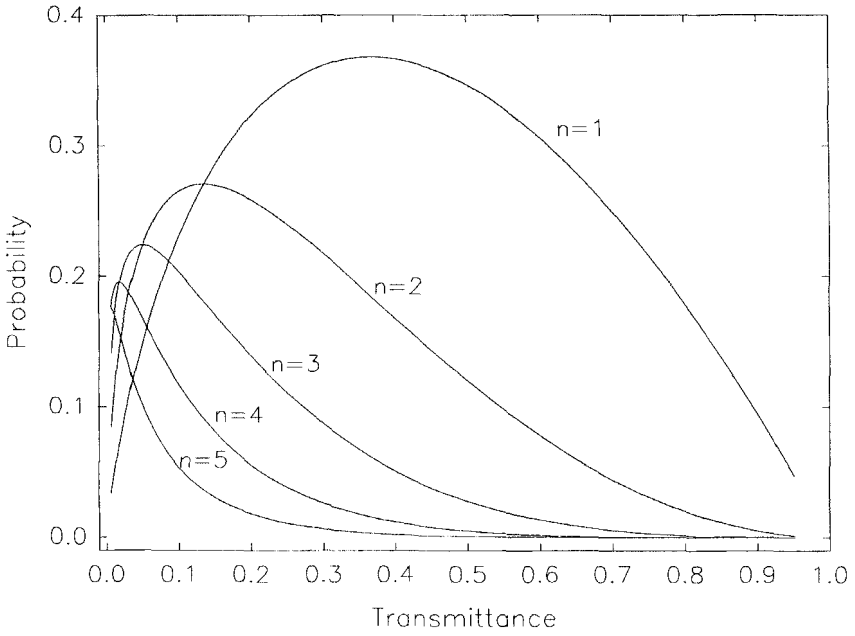

Figure 3. Multiple scattering probabilities.

distribution from 0 to 2π. For the ith order scattering, the outgoing wavevector $\mathbf{k}'$ is related to the incident wavevector $\mathbf{k}$ by

$$\mathbf{k}' = \left[\prod_{j=1}^{i} \mathbf{M}(\theta_j, \phi_j) \right] \cdot \mathbf{k}, \tag{11}$$

where matrix $\mathbf{M}(\theta, \phi)$ is the standard three dimensional rotation matrix

$$\mathbf{M}(\theta, \phi) = \begin{bmatrix} \cos\theta\cos\phi & -\sin\phi & \sin\theta\cos\phi \\ \cos\theta\sin\phi & \cos\phi & \sin\theta\sin\phi \\ -\sin\theta & 0 & \cos\theta \end{bmatrix}. \tag{12}$$

Array $I(\theta)$ stores the final multiple scattering pattern as a function of the polar angle θ.

The calculations were carried out on an IBM RS/6000 workstation with one million iterations for each transmittance value. The angular distribution of scattered light intensity is shown in figure 5 for different film transmittances, using the film-averaged cross-section for $kR = 13$, and ignoring the coherence effects of the structure factor. (If the droplet positions are truly random, the structure factor is unity for all $\mathbf{q}$.) The curves are normalized to give the same total scattered intensity when integrated over all solid angles.

No dependence on the azimuthal angle is predicted for the uniform director configuration.

3. The experiment

We studied the angular distribution of scattered light from PDLC films made with a 50/50 mixture of the liquid crystal E7 (Merck Ltd.) and the UV-curable epoxy

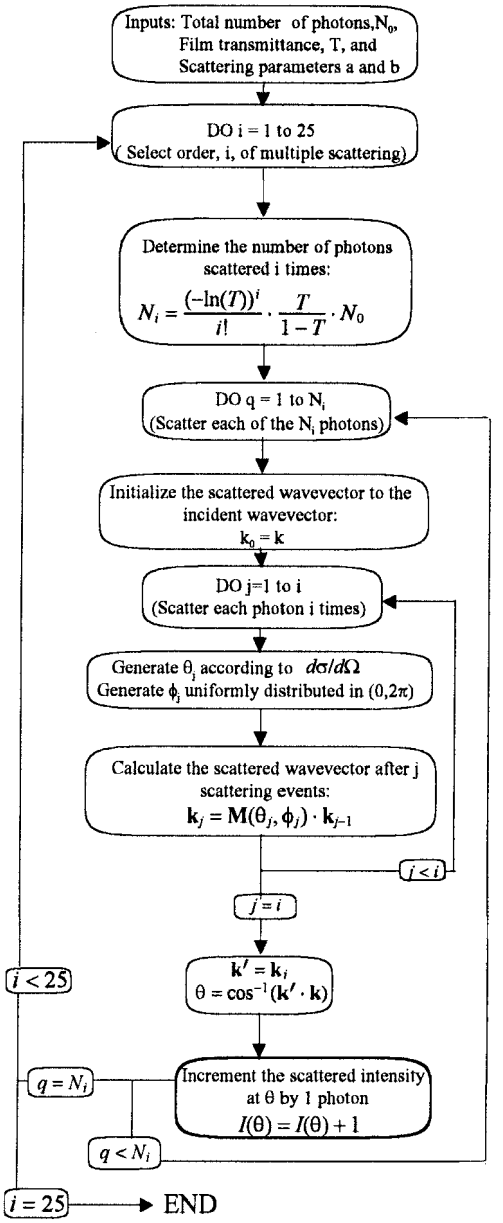

Figure 4. Flow chart of the multiple scattering Monte Carlo simulation program.

NOA65 (Norland). Films of nominal thicknesses of 5, 10, 16 and 25 μm were prepared between two ITO-coated glass substrates using glass fibre spacers. The same ultraviolet intensity of 3·4 mW cm^{-2} was used to prepare all samples. The average droplet radius had been previously determined from SEM to be 0·8 μm [8].

The light scattering apparatus consisted of a HeNe laser light with a polarized output beam. The light passed through a spatial filter and beam expander optics to produce a 0·5 cm spot at the sample. The beam was incident normal to the film in all cases. The scattered light was detected by a photodiode attached to a rotatable arm

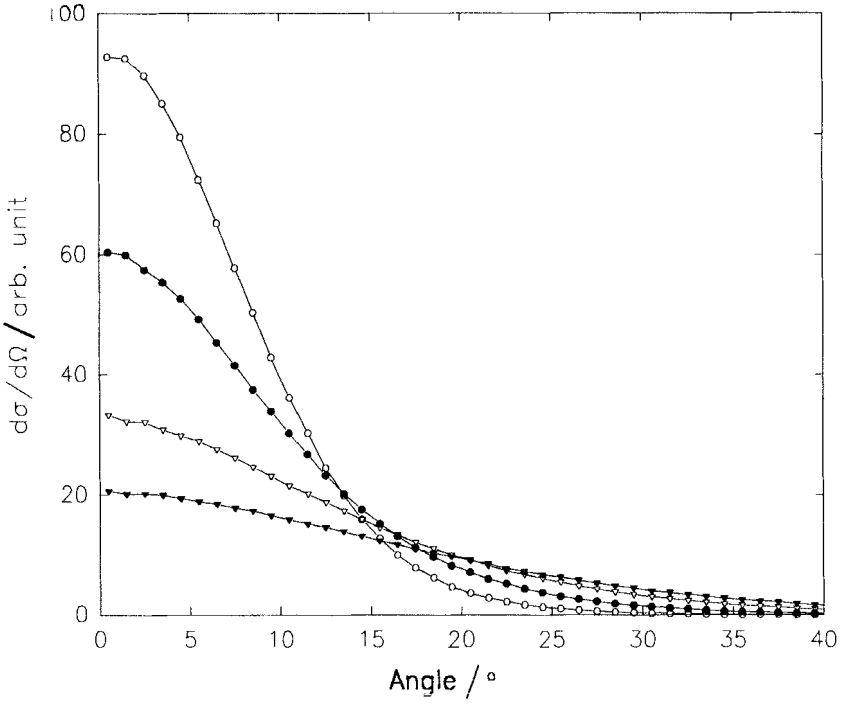

Figure 5. Monte Carlo simulation of multiple scattering patterns. All patterns are normalized to give the same total cross section. 1 000 000 iterations. ○, $T=50$ per cent; ●, $T=10$ per cent; ▽, $T=1$ per cent; ▼, $T=0{\cdot}1$ per cent.

that was driven by a stepper motor. A beam stop was used to block the transmitted beam; the stop subtended an angle of less than 0·5°.

To study the scattering in the presence of an electric field, a 1·0 kHz sinusoidal voltage of variable amplitude was applied to the ITO electrodes.

4. Results and discussion

For each film, the scattering profile was measured at four different values of transmittance: off state, 10, 50 and 90 per cent of the maximum. (The 5 μm sample was above 10 per cent transmissive in the off state, so only three curves are plotted.) The results are shown in figure 6. Here, the scattering (**kk**′) plane is orthogonal to the polarization of the incident beam.

Perhaps the most striking feature of the off state scattering is the intensity maximum for $|\mathbf{q}| \neq 0$. The maximum is most pronounced for the 5 μm sample and diminishes with increasing film thickness. The position of the peak is $\sim 8°$ for all samples. In contrast, the single droplet differential cross-section peaks at $\mathbf{q}=0$. This peaking of the scattering off axis indicates a **q** dependent structure factor (cf. equation (2)), and is commonly observed for a non-random distribution of particles [15, 16]. Apparently, this influence is mitigated by the multiple scattering in the thicker films. Multiple scattering destroys the coherence of the scattered fields.

In general, we found that the scattering does not have azimuthal symmetry. A two lobed pattern is observed that, again, is much more pronounced for the thinner

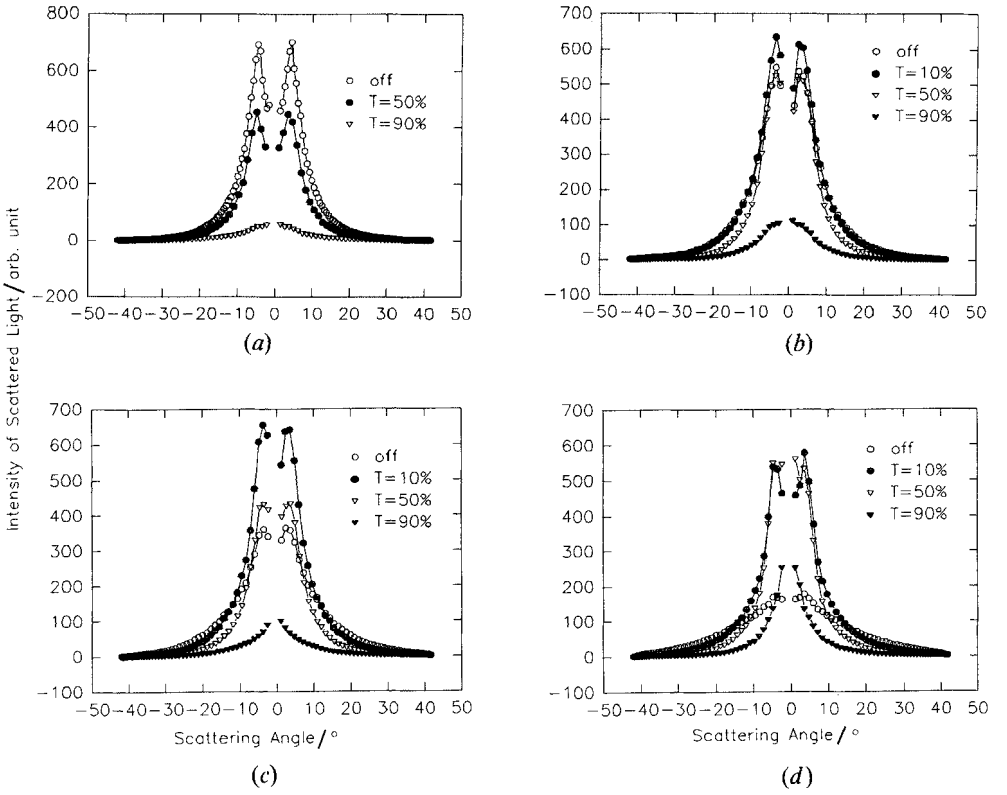

Figure 6. Angular distribution of scattered light for four different transmittance values. (*a*) 5 μm; ○, off state; ●, $T=50$ per cent; ▽, $T=90$ per cent. (*b*) 10 μm; ○, off state; ●, $T=10$ per cent; ▽, $T=50$ per cent, ▼, $T=90$ per cent. (*c*) 16 μm; ○, off state; ●, $T=10$ per cent; ▽, $T=50$ per cent, ▼, $T=90$ per cent. (*d*) 25 μm; ○, off state; ●, $T=10$ per cent; ▽, $T=50$ per cent, ▼, $T=90$ per cent.

samples, and weakens with applied field strength. Also the off axis maximum disappears when the polarization is perpendicular to the scattering plane (see figure 7). This behaviour results from the director configuration in the droplets; azimuthal symmetry is observed when the sample is heated into the isotropic phase. As noted previously, a uniform director configuration will not produce a two lobed scattering pattern, indicating that a scattering centre of lower symmetry is present. A bipolar configuration is most probable.

The scattering profile of the thicker films is clearly broadened by multiple scattering. The angular distribution of the scattered light agrees well with the model when there is little single scattering. Figure 8 compares the multiple scattering model to the scattering profile of the 25 μm film in the off state. The experimental curve was corrected for refraction at the air-glass interface. The only adjustable parameter for this fit was kR. (The curves were normalized to have the same total scattered flux.) $kR=13$ Corresponds to a droplet radius of 0·85 μm, in very close agreement with the SEM value. The single scattering profile is also shown in figure 8 and is markedly different from what is observed. Figure 9 shows a fit similar to figure 8 for the same film, only at 50 per cent transmittance. In this case, however, we fixed kR at the zero field value. Again the fit is quite good.

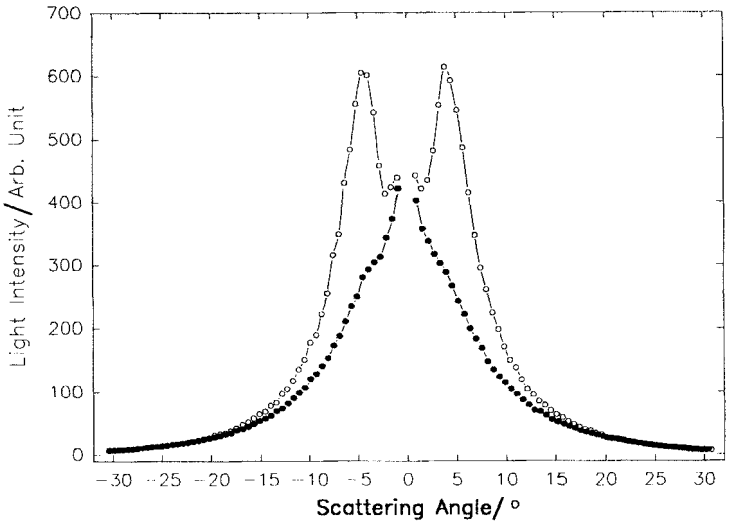

Figure 7. Angular distribution of scattered light for the 5 μm film in the off state, both perpendicular (●) and parallel (○) to the plane defined by the incident wave vector and polarization.

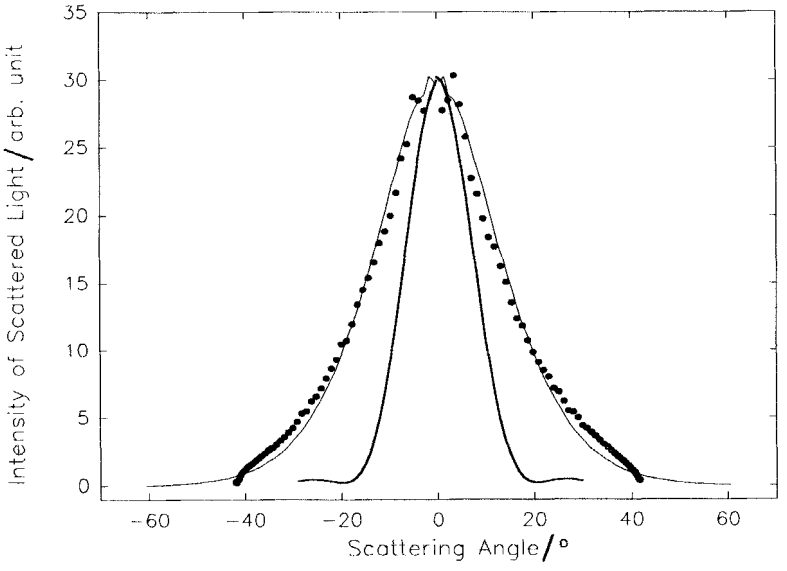

Figure 8. Angular distribution of scattered light for the 25 μm film in the off state (●), model (multiple scattering) (——), and model (single scattering) (——).

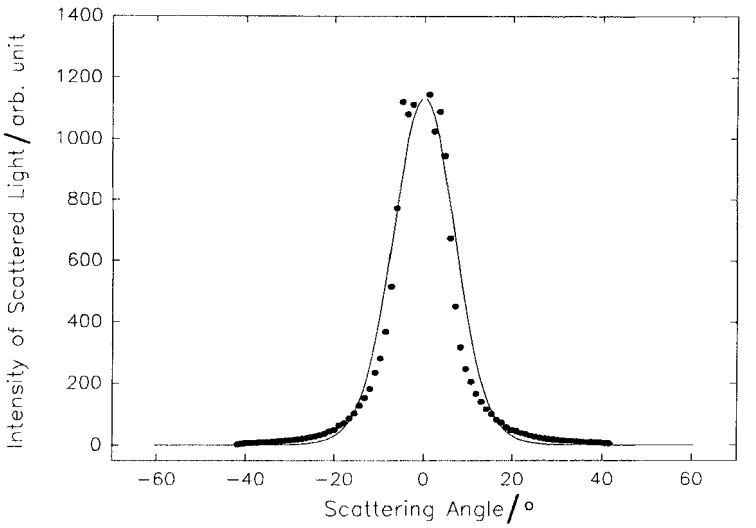

Figure 9. Angular distribution of scattered light for the 25 μm film in the 50 per cent transmissive state (●), and for the multiple scattering theory (——).

We should note that the fit is very sensitive to the choice of kR. For example, a kR of 12, corresponding to a droplet radius of 0·8 μm, gives a noticeably poorer fit. This is particularly true for higher transmittances, because the single scattering is highly dependent on kR.

Finally, we checked the model prediction that all curves have the same profile at fixed transmittance. We chose a 50 per cent transmittance for the comparison (see figure 10). The model prediction is born out in practice. Some deviations at small angles are observed because of the interference effects mentioned above, but the scattering at wider angles is nearly identical. Again, the curves are normalized to give the same total photon flux.

5. Conclusion

Multiple scattering plays a major role in defining the scattering characteristics of PDLC films. This is perhaps stating the obvious, but the consequences are not so apparent. Multiple scattering destroys the coherence of the scattered waves and broadens the angular distribution of the scattered light. However, even with this broadening, we find that the light is substantially scattered at small angles.

To achieve a complete description of the scattering it will be necessary to specify the detailed director configuration in the droplets, as well as the structure factor. Regarding the structure factor, we have found that neither the random distribution [7] nor the Percus–Yevick distribution for hard spheres [17, 18] provides a good description of the structure factor in PDLC films. Here, more work is needed.

Fortunately, for their application to projection displays, PDLC films with low off state transmissions are required. For those films, we find that coherence effects are significantly reduced. In this regime, the scattering model presented here gives a good qualitative and, in some respects, quantitative description of the scattering. In particular, the film-averaged differential cross-section, as determined from the droplet director distribution function, appears to be a useful concept. This model can be coupled with a model for the (possibly time-dependent) droplet director

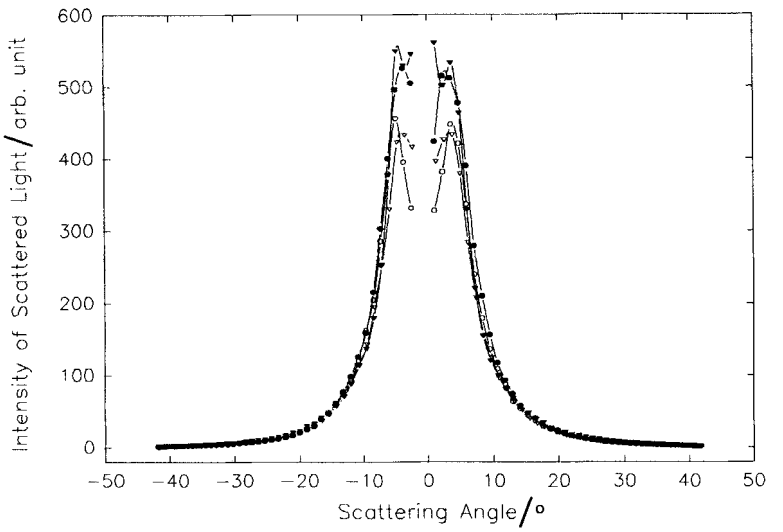

Figure 10. Angular distribution of scattered light for the four films at a common transmittance of 50 per cent. ○, 5 μm sample; ●, 10 μm sample; ▽, 16 μm sample; ▼, 25 μm sample.

distribution in the presence of a reorienting field [12]. In this way it will be possible to describe important static and dynamic quantities, such as the contrast ratio and switching speed, for realistic situations (i.e. $f/\# \neq \infty$).

This work was supported by grants from the National Center for Integrated Photonics Technology (NCIPT) under DARPA contract MDA972-90-0037 and the National Science Foundation under grant ECS-9020420.

References

[1] DRZAIC, P. S., 1986, *J. appl. Phys.*, **60,** 2142.
[2] DOANE, J. W., GOLEMME, A., WEST, J. L., WHITEHEAD, J. B., and WU, B.-G., 1988, *Molec. Crystals liq. Crystals*, **165,** 511.
[3] MONTGOMERY, G. P., JR., and VAZ, N. A., 1989, *Phys. Rev.* A, **40,** 6580.
[4] HIRAI, Y., NIIYAMA, S., OOI, Y., KUNIGAMA, M., KUMAI, H., YUKI, M., and GUNJIMA, T., 1990, *SPIE Proc.*, **1257,** 2.
[5] JONES, P., TOMITA, A., and WARTENBERG, M., 1991, *SPIE Proc.*, **1456,** 6.
[6] REAMEY, R. H., MONTOYA, W., and WARTENBERG, M., 1991, *SPIE Proc.*, **1455,** 39.
[7] ZUMER, S., GOLEMME, A., and DOANE, J. W., 1989, *J. opt. Soc. Am.* A, **6,** 403.
[8] KELLY, J. R., WU, W., and PALFFY-MUHORAY, P., 1992, *Molec. Crystals liq. Crystals*, **223,** 251.
[9] ZUMER, S., and DOANE, J. W., 1986, *Phys. Rev.* A, **34,** 3373.
[10] ZUMER, S., 1988, *Phys. Rev.* A, **37,** 4006.
[11] KIM, J. Y., and PALFFY-MUHORAY, P., 1991, *Molec. Crystals liq. Crystals*, **203,** 93.
[12] LI, Z., KELLY, J. R., PALFFY-MUHORAY, P., and ROSENBLATT, C., 1992, *Appl. Phys. Lett.*, **60,** 3132.
[13] KELLY, J. R., and PALFFY-MUHORAY, P., 1991, *ALCOM Symposium Series*, **1,** 1.
[14] VAN DE HULST, H. C., 1980, *Multiple Light Scattering*, Vol. I and II.
[15] PUSEY, P. N., and TOUGH, R. J. A., 1985, *Dynamic Light Scattering*, edited by R. Pecora (Plenum), p. 85.
[16] ZIMAN, J. M., 1979, *Principles of the Theory of Solids* (Cambridge University Press).
[17] PERCUS, J. K., and YEVICK, G. J., 1957, *Phys. Rev.*, **110,** 1.
[18] WERTHEIM, M. S., 1963, *Phys. Rev. Lett.*, **10,** 321.